HHS Public Access

Author manuscript

J Immunol. Author manuscript; available in PMC 2015 July 21.

Published in final edited form as:

J Immunol. 2014 April 15; 192(8): 3569–3581. doi:10.4049/jimmunol.1302766.

Axl receptor blockade ameliorates pulmonary pathology resulting from primary viral infection and viral exacerbation of asthma

Takehiko Shibata[*,1], **David M. Habiel**[*], **Ana L. Coelho**[*], **Steven L. Kunkel**[*], **Nicholas W. Lukacs**[*], and **Cory M. Hogaboam**[*,○,2]

[*]Immunology Program, Department of Pathology University of Michigan Medical School Ann Arbor, MI, 48109

[○]Division of Pulmonary and Critical Care Medicine, Department of Medicine Cedars-Sinai Medical Center Los Angeles, CA, 90048

Abstract

Viruses utilize Tyro3, Axl, and Mertk (TAM) receptor tyrosine kinases to infect and modulate the immune properties of various cell types leading us to investigate whether TAM receptor activation impacted primary viral infection and viral exacerbation of asthma in experimental models. In these lung-specific models, we observed that Axl was the most abundantly induced TAM receptor protein. During primary respiratory syncytial virus (RSV) infection, anti-Axl mAb treatment significantly increased the number of IFN-γ-producing T cells and NK cells, and significantly suppressed RSV replication and whole lung levels of IL-4 and IL-13. Intrapulmonary H1N1 infection induced lethal pulmonary inflammation but anti-Axl mAb treatment of infected mice significantly increased the number of IFN-β-producing macrophages and dendritic cells, and significantly suppressed neutrophil infiltration. Consequently, the lethal effect of H1N1 infection in this model was significantly reduced in the mAb-treated group compared with the IgG control-treated group. Targeting Axl also inhibited airway hyperresponsiveness, IL-4 and IL-13 production, and goblet cell metaplasia in an *Aspergillus fumigatus*-induced asthma model. Finally, infection of mice with RSV during fungal asthma significantly exacerbated airway inflammation, goblet cell metaplasia, and airway remodeling but all of these features in this viral exacerbation model were ameliorated by anti-Axl mAb treatment. Together, these results demonstrate that Axl modulates the pulmonary immune response during viral and/or allergic pathology, and also suggest that targeting this TAM receptor might provide a novel therapeutic approach in these infectious diseases.

Keywords

Axl; Mertk; Anti-monoclonal Axl antibody; RSV; Influenza virus; *Aspergillus fumigatus*; Asthma; Allergic inflammation

[1]Address Correspondence to: Takehiko Shibata, PhD Communicating author University of Michigan Medical School Room 4710, BSRB 109 Zina Pitcher Place Ann Arbor, Michigan, USA, 48109-2200. [2]**Cory M. Hogaboam, PhD** Cedars-Sinai Medical Center 8700 Beverly Blvd. AHSP Room A9408 Los Angeles. CA 90048.

Introduction

Viral pathogens that target the respiratory system typically evoke well-defined and unique innate immune responses, which in turn trigger specialized adaptive immune responses. The combination of these immune responses typically leads to the containment and clearance of the viral pathogen, and the establishment of long-term immunity. However, there is growing evidence that respiratory viruses usurp core elements of the immune response resulting in severe and prolonged inflammation, lung pathology, morbidity, and mortality (1, 2). One example is respiratory syncytial virus (RSV), which is a major cause of severe respiratory disease in infant and immunocompromised patients. Indeed, the World Health Organization estimates that RSV causes up to 64 million infections and 160,000 deaths annually (3). Further, pediatric RSV infection can markedly heighten the risk of subsequent recurrent wheezing and asthma, which is characterized by an inappropriate Th2-mediated immune response (4-8). Likewise, RSV infection in experimental models similarly leads to persistent airway inflammation and hyperresponsiveness (9-11), and this virus can also exacerbate asthma in any age group (12). Influenza virus type A is another example of a virus that is highly contagious and causes significant morbidity and mortality in mammals (13, 14). In 2009, H1N1 influenza spread worldwide (14), and in the United States alone, this strain of influenza virus affected 57 million Americans and caused 11,000 deaths. Influenza is another major viral pathogen that has been implicated in the exacerbation of asthma. Thus, strategies are required that both facilitate viral clearance and modulate the inflammatory responses that lead to susceptibility to these respiratory pathogens.

Tyro3, Axl, and Mertk (TAM) receptors belong to a distinct receptor protein-tyrosine kinase subfamily and are expressed in various cells and tissues. First described as critical receptors for the clearance of apoptotic cells and as pro-proliferative mediators on smooth muscle and fibroblasts, it is now known that TAM receptors have potent immune-modulating functions related to their induction of immunoregulatory factors including suppressor of cytokine signaling 1 (SOCS1), SOCS3, and Twist that inhibit both toll-like receptor (TLR)- and cytokine-driven immune responses (15-18). Vitamin K-dependent protein growth arrest-specific protein 6 (Gas6) and protein S are the two ligands that bind and activate the TAM receptor (19). More is known about Gas6, which is a soluble factor that binds to Axl and Tyro3 with equal affinity but binds Mertk with an affinity that is 3-10-fold lower (20-22). Although Gas6 and TAM receptors are detected in a variety of diseases and their roles are many and varied (23-28). A major focus of studies has been tumorigenesis and targeting Axl and Mertk suppresses tumor progression (29-33), since one role of TAM signaling is the induction of cell growth. However, recent studies have identified critical roles for TAM receptors in viral entry into target cells raising the possibility that targeting these receptors during primary and secondary pulmonary infection might be of therapeutic value (34-40).

Thus, the aim of the present study was to explore the expression and role of TAM receptors in experimental models of primary viral infection and virus-exacerbated allergic asthma. Given its relative abundance compared with the two other TAM receptors in these models, the specific role of Axl was explored using a mAb. Our data show that anti-Axl mAb treatment both attenuated viral infection and modulated the immune responses evoked during primary viral infection and virus-induced exacerbation of allergic asthma.

Interestingly, Axl contributed to both acute and chronic inflammatory and remodeling features in these models.

Material & Methods

Mice

Female, C57BL/6 mice (6 to 8 weeks of age) were purchased from Taconic Farms (Germantown, NY). Prior approval for mouse use in the protocols described below was obtained from the University Committee on Use and Care of Animals at the University of Michigan.

Primary respiratory syncytial virus (RSV) infection model

The Line 19 strain was originally isolated from a RSV-infected infant at the University of Michigan Hospital and was propagated in cultured HEp-2 cells (American Type Culture Collection) in the laboratory. Line 19 elicits disease in mice comparable to severe RSV infection in humans, including significant airway hyperresponsiveness and mucus overproduction (41). Groups of 5 mice were anesthetized and infected via intratracheal injection with 1×10^5 PFU/animal, and analyzed at days 3, 6, 9, and 12 after infection. In separate experiments, groups of 5 mice were treated via intraperitoneal injection with human IgG1 (i.e. control group; 5 μg/dose) or anti-Axl mAb (monoclonal anti-human Axl monoclonal antibody YW327.6S2; Genentech; 5 μg/dose). Note that the anti-Axl mAb recognizes both mouse and human Axl with high affinity (42).

Primary influenza virus infection (H1N1) model

Mice received an intranasal challenge with 3.0×10^3 PFU of influenza A virus strain (strain A/PR8/34; H1N1 isotype: ATCC) suspended in 40 μl of PBS. PBS was inoculated intranasally into mock-infected mice. In separate experiments, mice were injected into the peritoneal cavity with human IgG1 antibody (5 μg/dose) or anti-Axl mAb (5 μg/dose) prior to and on days 2, 4, 6, 8, and 10 after viral challenge. We also examined the therapeutic effects of anti-Axl mAb treatment in which groups of 5 mice were injected into the peritoneal cavity with human IgG1 antibody (5 μg/dose) or anti-Axl mAb (5 μg/dose) on days 2, 4, 6, 8, and 10 after H1N1 challenge. At days 2, 4, and 8 after infection, the left lung lobe was used for histological assessment, and the right lobes were used for the analysis of mRNA, protein, and flow cytometry.

Chronic fungal asthma in mice

Mice were sensitized with *Aspergillus fumigatus* antigens as previously described in detail (43). After Aspergillus sensitization, mice were challenged via oropharyngeal instillation of live, swollen *A. fumigatus* conidia. Beginning at day 14 after conidia challenge, other groups of mice received human IgG1 (5 μg/dose) or anti-Axl mAb (5 μg/dose) via i.p. instillation every other day until day 28 after conidia challenge. Similarly, beginning at day 14 after conidia challenge, other groups of mice received mouse IgG1 (5 μg/dose) or anti-Mertk mAb (5 μg/dose, Abcam, MA) via i.p. instillation every other day until day 28 after conidia challenge. At day 28 after *A. fumigatus* conidia, AHR was assessed in all groups of mice using a Buxco™ plethysmograph (Buxco, Troy, N.Y., USA). Briefly, sodium pentobarbital

(Butler, Columbus, Ohio, USA; 0.04 mg/g of mouse body weight) was used to anesthetize mice prior to their intubation and ventilation with a Harvard pump ventilator (Harvard Apparatus, Reno, Nev., USA). Once baseline airway resistance was established, 210 μg/kg or 420 μg/kg of methacholine were administered intravenously through a tail vein, and AHR was monitored for approximately 2 min. The peak increase in airway resistance was then recorded. After the assessment of AHR, whole lung lobes were dissected from each mouse and snap frozen in liquid nitrogen for genomic and proteomic analysis or fixed in 10 % formalin for histological analyses. Femur and tibia were also collected for the culture of various myeloid populations (see below).

RSV-induced exacerbation of fungal asthma in mice

At day 30 after Aspergillus conidia challenge, asthmatic mice were anesthetized and infected intratracheally with RSV (1×10^5 PFU/mouse). In separate experiments, mice were treated intraperitoneally with human IgG1 (5 μg/dose) or anti-Axl mAb (5 μg/dose) prior to and at days 2, 4, 6, 8, and 10 after RSV injection. At day 42 after conidia and day 12 after RSV infection, the left lung lobe was used for histological assessment, and the right lobes were used for the analysis of mRNA, protein, and flow cytometry in each mouse.

Bone marrow-derived DC and macrophage culture, isolation, and activation

Bone marrow-derived DCs or macrophages were prepared from naive or allergic mice at various times prior to and after conidia challenge in the latter group of mice. To generate DCs, bone marrow cells were cultured for 6 days with granulocyte-macrophage colony-stimulating factor (20 ng/ml; R&D Systems) and DCs were sorted for $CD11c^+$ expression using magnetic-activated cell sorting (Miltenyi Biotech, Bergisch Gladbach, Germany). To generate macrophages, bone marrow cells were cultured for 6 days with L-cell supernatant containing macrophage colony stimulating factor, and the resultant adherent cells were approximately 97.5% F4/80-positive macrophages as determined by flow cytometry. In additional experiments, bone marrow-derived DCs and macrophages were exposed to RSV at 1×10^4 PFU/ml or H1N1 virus at a MOI=10, and then incubated for 24 h before analysis.

Lung viral titers after H1N1 infection

To calculate viral titers, MDCK cells (1.5×10^4 /well) in MEM medium with 10% FCS were added to 96-well microplates and were incubated at 37°C in a humidified atmosphere with 5% CO_2 for overnight. On day 2, supernatants from H1N1-infected lung were prepared in MEM and MDCK cells were washed twice with PBS prior to the addition of 100 μl of supernatant in triplicates. After 1 h of exposure, virus suspensions were removed and the cells were washed twice with PBS. MDCK cells were incubated at 37°C in a humidified atmosphere with 5% CO_2 for an additional 3 days. Then, MDCK cells were washed twice with PBS, and 100 μl of MEM without phenol red (Sigma-Aldrich, MO) and 50 μl of XTT based (Sigma-Aldrich), sodium3'-[1-[(phenylamino)-carbonyl]-3,4-tetrazolium]-bis(4-methoxy-6-nitro) benzene-sulfonic acid hydrate were added to each well. After 4 h of incubation at 37°C, the absorbance at 450 nm was measured. Finally, to calculate the changes of viral titers between the antibody treatment groups, the absorbance of supernatant from MDCK cells exposed to IgG-treated lung supernatants at day-2 after H1N1 infection were assigned a value of 1 and the reciprocal number of each group were shown.

Quantitative PCR analysis

Total RNA was isolated from whole lung or cultured cells using Trizol reagent (Invitrogen/Life Technologies, Carlsbad, CA). Purified RNA was treated with DNase, and 0.2 μg of RNA was reverse transcribed into cDNA using TaqMan reverse transcription reagents (Foster City, CA). Quantitative gene expression assays were used to quantify *Tyro3*, *Axl*, *Mertk*, *Il1b*, *Il6*, *Tnfα*, *Il4*, *Il5*, *Il10*, *Il13*, *Ifnα1*, *Ifnβ*, *Ifnγ*, *Rsv-g*, *Cxcl2*, *Ccl2*, *Fizz1*, *Muc5ac*, *Gob5*, *Tgfβ1*, *Col1a1*, *Col3a1*, and *Gas6* according to the manufacturer's directions (Applied Biosystems, Carlsbad, CA). The fold changes in transcript expression were calculated by comparing the gene expression in whole lung or cell culture samples to that of transcript levels in naïve whole lung or control cell conditions, and the levels in the latter two types of samples were assigned a value of 1.

Whole lung immunohistochemical and histological analysis

Whole lungs were fully inflated with 10% formalin, dissected, and placed in fresh 10% formalin for 24 h. Routine histological techniques were used to paraffin embed the entire lung, and 5 μm sections of whole lung were analyzed by immunohistochemical (IHC) techniques. Briefly, 5-μm histological sections were dewaxed with xylene, rehydrated in graded concentrations of ethanol, and a rabbit anti-mouse Axl polyclonal antibody (Lifespan BioSciences, Inc., WA) or a rabbit anti-mouse Mertk polyclonal antibody (Lifespan BioSciences, Inc., WA) was used for Axl and Mertk expression, respectively. Other tissue sections were exposed to control IgG isotype antibody. A mouse horseradish peroxidase–diaminobenzidine cell and tissue-staining kit was then used according to the manufacturer's instructions (R&D Systems, MN) to develop each slide. Additional tissue sections were stained with one of hematoxylin and eosin (H&E), Periodic acid-Schiff (PAS; to detect mucus cell metaplasia), or Masson trichrome (to detect collagen).

Flow cytometry analysis

Whole lung samples incubated with collagenase (1 mg/ml, Roche, Mannheim, Germany) at 37°C for 45 min. Whole lung cell suspensions were then incubated with anti-CD16/32 (2.4G2) and further labeled with fluorescent dye-conjugated mAb (CD45, CD11b, F4/80, CD11C, Ly6C, Ly6G, CD3, CD4, CD8, NK1.1; eBioscience, San Diego, CA) for 30 min. Tissue culture-generated cells were incubated with the same antibodies for the same amount of time. For intracellular staining of cytokines, lung cells (1.0×10^6 cells/well) were cultured in 48-well plates containing plate-bound anti-CD3 (5 μg/ml) and soluble anti-CD28 (2.5 μg/ml). After overnight incubation and in the presence of GolgiPlug (BD Biosciences-Pharmingen) for the last 2 h at 37°C and 5% CO_2, the cells were stained for surface markers with anti-CD4, anti-CD8, or anti-NK1.1 Abs, re-suspended in fixation/permeabilization solution (BD Cytofix/Cytoperm Kit; BD Biosciences Pharmingen), and stained with anti-IFN-γ or anti-IFN-β Abs (PBL Interferon Source, NJ) for 30 min. Data were acquired on an LSRII machine by using FACSDiVa software (BD Biosciences), and all data were analyzed using a FlowJo software package (TreeStar, Inc., Ashland, OR).

ELISA and Bioplex Analysis

Murine IL-4, IL-10, IL-13, and IFN-γ were measured in whole lung or tissue culture samples using a standardized sandwich enzyme-linked immunosorbent assay (ELISA, R&D system) or a bead-based multiple target sandwich ELISA system (BioPlex; BioRad Laboratories, Hercules, CA). Recombinant murine proteins (R&D Systems) were used to generate standard curves. The limit of ELISA detection for each cytokine was consistently > 15.6 pg/ml for each sandwich ELISA and 1 pg/ml for BioPlex. The cytokine and chemokine levels in each lung homogenate sample were normalized to total protein levels, which were measured using the Bradford assay.

Statistical analysis

All results are expressed as the mean ± SEM. A Student's *t*-test or an analysis of variance and a Student-Newman-Keuls multiple comparison test were used to determine statistical significance between groups. $P \leq 0.05$ was considered statistically significant.

Results

TAM receptor expression following primary RSV infection

Primary RSV infection induced transcript levels of all three TAM receptors in the lung after virus infection (**Fig. 1A**). However, immunohistochemical analysis of whole lung samples from RSV-infected mice revealed that Axl was the most prominently induced TAM receptor at the protein level particularly in lung resident alveolar and interstitial macrophages, and in airway epithelial cells (**Fig. 1B**). Mertk protein appeared to be constitutively expressed in both macrophages and epithelial cells, and the expression of this TAM receptor appeared to be further induced in epithelial cells at days 12 after RSV infection. To confirm that RSV infection altered TAM receptor expression in cells of myeloid origin, macrophages and dendritic cells were cultured using bone marrow cells removed from naïve mice. When bone marrow-derived macrophages (BMDM) were exposed to RSV, Axl but not Mertk transcript expression was significantly increased (**Fig. 1C**). In contrast, neither Axl nor Mertk were increased in bone marrow-derived dendritic cells (BMDC) after their exposure to RSV (**Fig. 1D**). Interestingly, transcript levels of Gas6 appeared to be suppressed in both BMDM and BMDC following RSV exposure (**Fig. 1C & D**). Thus, pulmonary RSV infection induced Axl expression particularly in macrophages.

Axl facilitates infection and lung pathology after primary RSV infection

To investigate the role of Axl during primary RSV infection, we targeted this TAM receptor using a mAb (42). Naïve mice were treated every day with anti-Axl mAb beginning at two hours before infection and every other day until day 12 after RSV infection. Targeting Axl in this manner did not alter TAM receptor and Gas6 transcript expression in whole lung samples over the course of RSV infection. It was apparent in hematoxylin & eosin (H & E)-stained whole lung sections, primary RSV infection was associated with profound peribronchial inflammation that peaked at day 6 after infection in the IgG1 control group (**Fig. 2A**). In contrast, anti-Axl mAb treatment significantly suppressed the airway inflammatory response at this same time after RSV infection. Further, the anti-Axl mAb

treatment markedly reduced total cell numbers in bronchoalveolar lavage fluid (BALF) at days 3 after RSV infection (**Fig. 2B**). Morphologic analysis of BALF samples revealed that both neutrophil and monocytes/macrophages numbers were significantly lower at day 3 after RSV infection (**Fig. 2B & C**). Primary RSV infection induced Th2 cytokines including IL-4 and IL-13 at day 6 after RSV infection (**Fig. 2D**). Although the anti-Axl mAb treatment did not affect pro-inflammatory cytokines such as IL-1β, IL-6, and TNF-α at anytime after RSV infection, this treatment significantly decreased whole lung IL-4 and IL-13 levels compared with the IgG1 control group at day 6 after RSV infection (**Fig. 2D**). Further, unlike the control IgG1 group, the expression of IFN-γ, but not IFN-α and IFN-β, protein was significantly increased in the anti-Axl mAb treatment group at day 9 after RSV infection (**Fig. 2E**). Importantly, the anti-Axl mAb treatment significantly inhibited RSV replication compared with the IgG1 control group as revealed by the significantly lower levels of *RSV-g* in whole lung samples in the anti-Axl mAb group (**Fig. 2F**). To further explore the source of IFN-γ in Axl targeted mice, various lung immune cells were analyzed at day 9 after RSV infection. Anti-Axl mAb treatment during RSV infection increased the number of IFN-γ-producing CD4 positive T cells and NK cells when compared to similar cell types in the control IgG1 group (**Fig.2 G&H**). Thus, these data demonstrated that Axl modulated both the intensity of the pulmonary RSV infection and the corresponding inflammatory response evoked by this virus.

TAM receptor expression following primary H1N1 infection

Influenza virus infection elicits a severe inflammatory response in the respiratory system of its host, thereby promoting significant morbidity and mortality. In the present study, transcript levels of all three TAM receptors were altered in whole lung samples at various times examined after primary H1N1 infection (**Fig. 3A & Supplemental Fig. 1B**). Again, the protein levels of Axl were increased particularly in myeloid cells and structural cells such as alveolar epithelial cells after H1N1 infection (**Fig. 3B**). We next investigated whether H1N1 infection altered Axl expression in myeloid cells such as macrophages and dendritic cells *in vitro*. H1N1 infection significantly induced Axl, but not Mertk transcript levels in BMDM compared with uninfected BMDM, while H1N1 infection suppressed Axl, Mertk, and Gas6 transcript expression in BMDC (**Fig. 3C**). Gas6 transcript was not increased in BMDM and BMDC following exposure to H1N1 *in vitro*. Together, these data indicated that H1N1 infection altered TAM receptor infection in a cell-specific manner.

Axl contributes to H1N1-induced lung pathology and mortality

H1N1 infection in mice elicits a lethal pulmonary inflammatory response. In the IgG1-treated control group, mice began to die at day 7 after H1N1 infection, and all mice in this control group were dead by day 9 after infection (**Fig. 4A**). Conversely, treatment of another group of H1N1-infected mice with anti-Axl mAb significantly reduced the lethal effect of this virus, and 60% of these antibody-treated mice were alive at day 12 after infection (**Fig. 4A**). While targeting Axl in the H1N1 infection model, significantly decreased Tyro3 transcript levels at day 3 of infection compared with the IgG1 group, this TAM receptor was similar in both groups at all other times after infection (**Supplemental Fig. 1B**). Further, Axl, Mertk, and Gas6 transcript levels were similar between the anti-Axl mAb and IgG1

treatment groups at all times after H1N1 infection (**Supplemental Fig. 1B**). As shown in **Fig. 4B**, H & E-stained whole lung samples revealed that H1N1 infection induced a severe pulmonary inflammatory response that appeared to increase in time-dependent manner. Conversely, anti-Axl mAb treatment dramatically inhibited this inflammatory response at all times examined in this model (**Fig. 4B**). Analysis of BALF revealed that the H1N1-induced pulmonary inflammatory response was dominated by neutrophils (**Fig. 4C & D**) and the numbers of these granulocytes were significantly reduced in anti-Axl mAb-treated mice (**Fig. 4D**). Consistent with these findings, H1N1 infection strongly induced whole lung transcript levels of inflammatory cytokines such as IL-1β, IL-6 and TNF-α in the control group. Anti-Axl mAb treatment significantly inhibited TNF-α, whereas transcript levels of both IL-4 and IL-10 were significantly increased in whole lung samples at day 2 after H1N1 infection compared with the IgG1 control group (**Fig. 4E**). Using flow cytometry, we also observed that the anti-Axl mAb treatment significantly inhibited the number of neutrophils but not other inflammatory cell types in H1N1-infected mice (**Fig. 4F & G**). The inhibition in lung neutrophil numbers also coincided with significantly reduced CXCL2 levels in the anti-Axl mAb-treated group versus the IgG1 control group (**Fig. 4H**).

To further explore the effect of Axl on the pulmonary innate immune response directed against H1N1, we next examined the effect of the anti-Axl mAb treatment on the generation of IFN-β, which is an important anti-viral cytokine against influenza virus. Whole lung samples from the anti-Axl mAb-treated group expressed significantly greater transcript levels of this cytokine at day 2 after H1N1 infection compared with the IgG1 group (**Fig. 4I**). The H1N1 titer at day-4 was significantly suppressed by anti-Axl mAb-treatment compared with the IgG treatment group (**Fig. 4J**). Cellular sources of IFN-β included macrophages and dendritic cells, and the *in vivo* anti-Axl mAb treatment significantly increased IFN-β production in isolated primary, interstitial macrophages and DCs (**Fig. 4K & L**). In H1N1-infected mice, $CD4^+$ T cells were identified as the primary source of IFN-γ but there was no significant difference between the IgG1 and anti-Axl mAb-treated groups (data not shown). Finally, we examined the therapeutic effect of anti-Axl mAb treatment administered to mice at days 2, 4, 6, 8, & 10 after H1N1 infection. When administered in this manner, the anti-Axl mAb treatment significantly improved mouse survival, improved lung histopathology, reduced neutrophil recruitment and viral titers compared with IgG1-treated mice (**Supplemental Fig. 2A-E**). Thus, targeting Axl directly modulated the immune response directed against H1N1, and enhanced survival in a murine model.

TAM receptor expression in chronic fungal asthma

Before exploring the impact of viral exacerbation in a fungal asthma model, we first examined whether TAM receptors were present and active in *A. fumigatus*-sensitized and conidia challenged mice. Whole lung Axl and Mertk, but not Tyro3 (not shown) transcript levels were significantly increased at day 28 after conidia challenge when compared with naïve mice (**Fig. 5A**). Consistent with the q-PCR findings, the number of Axl- and Mertk-positive cells was increased at day 28 after conidia challenge but Axl protein levels were markedly higher than Mertk protein levels (**Fig. 5B**). Specifically, airway epithelial cells and inflammatory lung myeloid cells strongly expressed Axl in whole lung tissue at day 28 after conidia (**Fig. 5B**). Using BMDM that were generated from naïve and asthmatic mice at days

7 or 28 after conidia, macrophages were explored as a putative source of Axl and Mertk. Compared with BMDM cultured at the other two time points, BMDM from asthmatic mice at day 28 after conidia significantly expressed inflammatory zone 1 (Fizz1; a marker for M2 macrophages), Axl, and Mertk (**Fig. 5C**). In addition, naïve BMDM that were M2-activated with IL-4 and IL-13 expressed significantly greater Fizz1, Axl, and Mertk compared with naïve BMDM that were M1-skewed with LPS and IFN-γ (**Fig. 5D**). Together, these data demonstrated that structural and myeloid-derived cells including macrophages exhibited dynamic Axl and Mertk expression in a chronic fungal asthma model.

Role of Axl in chronic fungal asthma

To determine the role Axl in this fungal asthma model, anti-Axl mAb was administered by i.p. injection every other day from days 14 to 28 after conidia to coincide with increased expression of this TAM receptor. Anti-Axl mAb treatment during this time significantly reduced methacholine-induced airway hyperresponsiveness (AHR) when compared with IgG1-treated controls (**Fig. 6A**). The peribronchial accumulation of inflammatory cells observed in histological tissue sections (**Fig. 6B**) and the number of cells in BALF (**Fig. 6C**) were significantly inhibited by the anti-Axl mAb treatment. Whole lung IL-4 and IL-13 levels were also significantly lower in the anti-Axl mAb-treated whole lung compared with the IgG1 group (**Fig. 6D**). Qualitative (**Fig. 6E**) and quantitative (**Fig. 6F**) analysis of histological tissue sections revealed that goblet cell metaplasia was reduced in the anti-Axl mAb group compared with the IgG1 group. Quantitative PCR analysis of whole lung RNA revealed that Gob5 transcript expression was significantly lower in the anti-Axl mAb-treated group compared with the IgG1 group (**Fig. 6G**). Targeting Axl in this manner significantly reduced transcript levels of Tyro3 compared with the IgG1 treatment group at day 28 after conidia but Axl, Mertk, and Gas6 transcript levels did not differ between these groups at the same time after conidia (**Supplemental Fig. 1C**). Because Mertk was also induced in a time-dependent manner in this fungal asthma model, we also examined the effect of an anti-Mertk mAb administered from days 14 to 28 after conidia. Unlike the results we obtained after targeting Axl in this model, the anti-Mertk mAb treatment had no affect on AHR, whole lung cytokine levels, peribronchial inflammation, goblet cell metaplasia, BALF cell counts, and whole lung transcript levels of mucus genes *Gob5* and *Muc5ac* (**Supplemental Fig. 3A-E**). Thus, antibody-mediated blockade of Axl inhibited both airway inflammatory and remodeling responses in a murine model of fungal asthma.

Role of Axl in RSV-exacerbated fungal asthma

RSV is one of many recognized viral pathogens that exacerbate allergic asthma. We hypothesized that viral exacerbation in asthma might be a consequence of enhanced Axl expression and function. Consistent with this hypothesis, *in vitro* studies showed that Poly I:C activation of naïve and asthmatic BMDM significantly increased Axl but not Mertk transcript expression compared with appropriate control cultures of BMDM (**Supplemental Fig. 4A**). Naïve BMDM skewed under M2 conditions also exhibited significantly higher Axl expression following their exposure to Poly I:C compared with cultures not exposed to Poly I:C (**Supplemental Fig. 4B**). To determine the role of Axl during RSV-induced exacerbation of fungal asthma, RSV was administered to asthmatic mice at day 30 after

conidia challenge, and anti-Axl mAb was administered immediately prior to and up to 10 days after the RSV challenge. At day 12 after RSV infection and day 42 after conidia, methacholine-induced AHR was significantly inhibited in the anti-Axl mAb-treated group compared with the IgG1-treated asthmatic group with RSV (**Fig. 7A**). Likewise, the RSV-induced peribronchial accumulation of cells (**Fig. 7B**) and presence of inflammatory cells in the BALF (**Fig. 7C**) were significantly lower in the anti-Axl mAb treatment group compared to control IgG1 group. In addition, the anti-Axl mAb treatment significantly increased whole lung IFN-β levels at day 12 after the RSV challenge of asthmatic mice (**Fig. 7D**). Further, the presence of RSV g-antigen in whole lung samples was significantly lower in the anti-Axl mAb-treated group compared with the IgG1-treated group (**Fig. 7E**). PAS staining in whole lung sections was also significantly lower and mucus gene expression was lower in anti-Axl mAb-treated asthmatic mice challenged with RSV compared with the similarly challenged group that received IgG1 (**Fig. 7F, G &H**). RSV infection also exacerbated peribronchial fibrosis as determined by quantification of collagen around airways, TGF-β production, and the expression of *Col1a1* and *Col3a1* in this asthma model, which was inhibited by the anti-Axl mAb but not the IgG1 treatment (**Fig. 7I & J**). Finally, anti-Axl mAb treatment reduced Axl but not Mertk expression in whole lung samples from asthmatic mice with RSV infection (**Supplemental Fig. 4C**). Thus, these data demonstrated that Axl contributed to RSV-exacerbated fungal asthma.

Discussion

The respiratory system is particularly susceptible to a number of viral pathogens, which cause significant morbidity and mortality due to their direct injury to lung cells and/or modulatory effects on the pulmonary mucosal immune response (44). Recent attention has been directed toward Gas6/TAM receptor interactions as a mode of viral entry into target cells (38). In addition, this ligand/receptor interaction is known to exert modulatory effects on TLR-induced immune activation, particularly in bone marrow-derived myeloid cells (15). In the present study, we primarily examined the role of the TAM receptor Axl in various murine models of primary and secondary viral infection in the lung. Compared with Mertk and Tyro3, Axl was the most consistently and strongly induced TAM receptor in macrophages and epithelial cells during primary viral infection, fungal asthma, and viral exacerbation of fungal asthma. Although several individual and combination TAM receptor gene-targeted mice strains are available, all of these adult mice exhibit major immune anomalies that precluded their use in the models used herein (15, 45, 46). Instead, we used mAbs directed against either Axl (42) or Mertk (47) to address the endogenous role of individual TAM receptors in WT mice. Targeting Axl via this biologic approach inhibited the adverse consequences of RSV and H1N1 infection in naïve mice, attenuated allergic inflammation and remodeling in a fungal asthma model, and blocked RSV-induced exacerbation of fungal asthma. Mechanistically, the blockade of Axl enhanced the innate anti-viral immune response in the lung via effects on type 1 IFN generation and, conversely, inhibited the Th2-driven allergic inflammatory responses in the asthmatic lung. Together, these data highlight the major role *in vivo* for Axl in regulating both innate and adaptive immune responses in the respiratory system.

The elucidation of effective and safe strategies for attenuating the adverse consequences of RSV infection remains a focus of considerable research attention (48). Strategies that most effectively promote beneficial innate immune responses against this non-lytic virus are believed to be more likely to succeed in the clinic but the key regulators of this type of immune response have yet to be uncovered (44). In the present study, targeting Axl with a mAb that binds to this receptor with high affinity and blocks the ability of Gas6 to signal (42) markedly reduced the histopathology typically evoked by RSV infection in naïve mice. The Line 19 strain of RSV used in the present study has been shown to promote the generation of Th2-type cytokines such as IL-4 and IL-13 (12) but we observed that targeting Axl significantly increased whole lung numbers of IFN-γ–expressing CD4+ T cells and NK cells compared with whole lung samples from the IgG1 treatment group. The increased Th1-type immune response in anti-Axl mAb-treated mice also coincided with enhanced viral clearance (i.e. lower RSV-g expression). These data are consistent with previous reports showing that Axl and Mertk double-deficient macrophages and DCs promote a Th1-type immune response (45), and TAM receptor activation in DCs inhibits Th1-type cytokine responses (49). Thus, Axl receptor blockade modulated the innate immune response directed against RSV in naïve mice leading to faster resolution of the viral infection and markedly reduced the subsequent tissue pathology.

Given its lytic effects on airway epithelial cells, H1N1 influenza infection induces a markedly more severe respiratory response compared with that evoked by RSV. While neutrophils are very important for the clearance of influenza virus from the lung, these cells can also contribute to the tissue pathology via cytotoxic effects on lung resident cells (50). In the present study, neutrophil influx into the H1N1-infected lung was a key histopathologic feature at day 4 after infection, and appeared to be one explanation for the 100% mortality observed in the control group. Conversely, H1N1-infected mice treated with anti-Axl mAb were protected from the lethal effects of this virus and this coincided with significantly fewer neutrophils both in the alveolar space and in the lung tissue compared with the IgG1-treated group. Significantly higher levels of IFN-β, IL-4, and IL-10, and significantly lower levels of TNF-α, and CXCL2 were also observed in the anti-Axl mAb-treated group compared with the IgG1-treated control group. More notably, targeting Axl worked in a therapeutic manner (in which administration of this mAb began 2 days after the H1N1 infection) to significantly attenuate H1N1-induced mortality. Presumably this therapeutic effect of the anti-Axl mAb treatment was due, in part, to the attenuation in neutrophil accumulation in BALF and lung tissue compared with the IgG1-treated group. IFN-β has a critical role in both the clearance of influenza virus and the resolution of inflammation after viral clearance (51), and the data presented herein suggest that targeting Axl leads to augmented generation of this potent anti-viral type 1 IFN in both interstitial macrophages and DCs. Thus, targeting Axl modulated the immune response elicited by H1N1 in the mouse respiratory system.

Dynamic changes in TAM receptor expression were observed during the development of adaptive immunity in an experimental asthma model. Transcript and protein levels of Axl and Mertk were significantly elevated in whole lung samples but only at day 28 after conidia in contrast to Tyro3, which showed decreased expression with time. We observed that both non-immune (i.e. airway epithelial cells, stromal cells, and vascular endothelial cells) and

immune cells (i.e. macrophage) in the lung increased Axl and Mertk expression during the course of this fungal asthma model, and these findings are consistent with previous reports demonstrating that various non-immune and immune cell types express both TAM receptors (52, 53). Anti-Axl, but not anti-Mertk, mAb treatment from days 14 to 28 after conidia significantly inhibited all features of experimental fungal asthma, which include peribronchial inflammation, methacholine-evoked AHR, and airway remodeling. One explanation for the failure of the anti-Mertk mAb therapy in this model is that, unlike Axl, Mertk has a major anti-inflammatory role via its use by myeloid cells to clear apoptotic cells, thereby leading to the generation of inflammation-resolving cytokines such as IL-10 (54-58). It is conceivable that the blockade of Axl might have enhanced Gas6/Mertk interactions consequently modulating the asthmatic response but changes in whole lung Mertk levels in anti-Axl mAb-treated mice do not fully support this hypothesis. Various soluble and cellular factors contribute to the development of AHR in fungal asthma but it is widely accepted that Th2-mediated immune events are the major drivers of this response (59, 60). Therapeutic anti-Axl mAb treatment suppressed AHR in a fungal asthma model and this coincided with significantly decreased Th2-type cytokine levels compared with the IgG1 treatment group. Interestingly, targeting Axl signaling inhibited IL-4 and IL-13 protein levels in the primary RSV infection model as well as the fungal asthma model. Future studies will be directed at the manner in which Axl activation promotes Th2 responses but the most likely mechanism involves SOCS3, which is induced by Axl signaling and has an important role in inducing Th2-type responses during asthma (15, 61). Together, these data demonstrate that targeting Axl inhibits the Th2-type immune response that is critically important for the airway inflammatory and remodeling features of experimental fungal asthma.

RSV infection in the experimental fungal asthma model caused severe inflammation, goblet cell hyperplasia, and airway remodeling. A number of immune factors probably contribute to viral exacerbation in asthma but Aoki and colleagues (62) discovered that Gas6 was one of 4 factors that were differentially expressed during asthma exacerbation. Although the administration of anti-Axl mAb from days 30 to 40 after conidia challenge had a modest effect on the fungus-driven features at day 42 in this model, this treatment had a readily apparent inhibitory effect on viral exacerbation of fungal asthma at the same time after conidia. A smaller quantity of anti-Axl mAb was administered in this asthma exacerbation model compared with the asthma model alone, perhaps explaining the lack of attenuation observed in the former. Nevertheless, anti-Axl mAb treatment in the asthma exacerbation model promoted an anti-viral innate immune response directed at RSV that was characterized by increased IFN-β. As in the primary RSV infection model, anti-Axl mAb treatment completely inhibited RSV-g levels in whole lung samples in the RSV exacerbation model. RSV-g protein is believed to induce the release of large amounts of Th2-type cytokines from $CD4^+$ T cells, mast cells, basophils, and monocytes thereby triggering increased pulmonary eosinophilia and asthma exacerbation (63). Targeting Axl clearly attenuated all histologic features of viral exacerbation of fungal asthma as demonstrated by significantly less peribronchial inflammation, mucus cell metaplasia, and peribronchial fibrosis in the anti-Axl mAb group compared with the IgG1 control group. Another key finding from the viral exacerbation model pertained to the prominent inducing effect of

dsRNA on the expression of Axl but not Mertk in BMDM generated from asthmatic mice. These data suggest that RSV infection during asthma can further enhance Axl expression thereby leading to exacerbated fungal asthma.

In summary, we have demonstrated that the TAM receptor Axl has a major role during primary and secondary viral infections in the respiratory system. The blockade of this receptor via a biologic approach revealed that Axl regulates key innate and adaptive immune responses in the lung that facilitate both viral infection and immunopathology. Together, these data suggest that targeting Axl receptor might provide an effective clinical therapy in virus-driven and/or exacerbated pulmonary disease.

Supplementary Material

Refer to Web version on PubMed Central for supplementary material.

Abbreviations

BMDC	Bone marrow-derived dendritic cells
BMDM	Bone marrow-derived macrophages
Gas6	Growth arrest-specific protein 6
H1N1	Influenza A
mAb	Monoclonal antibody
RSV	Respiratory syncytial virus
SOCS	Suppressor of cytokine signaling
TLR	Toll-like receptor
Twist	Twist proteins
TAM	Tyro3, Axl, and Mertk

References

1. Thompson WW, Shay DK, Weintraub E, Brammer L, Cox N, Anderson LJ, Fukuda K. Mortality associated with influenza and respiratory syncytial virus in the United States. JAMA. 2003; 289:179–186. [PubMed: 12517228]
2. Thompson WW, Shay DK, Weintraub E, Brammer L, Bridges CB, Cox NJ, Fukuda K. Influenza-associated hospitalizations in the United States. JAMA. 2004; 292:1333–1340. [PubMed: 15367555]
3. Collins PL, Graham BS. Viral and host factors in human respiratory syncytial virus pathogenesis. J Virol. 2008; 82:2040–2055. [PubMed: 17928346]
4. Silvestri M, Sabatini F, Defilippi AC, Rossi GA. The wheezy infant -- immunological and molecular considerations. Paediatr Respir Rev. 2004; 5(Suppl A):S81–87. [PubMed: 14980249]
5. Glezen WP, Taber LH, Frank AL, Kasel JA. Risk of primary infection and reinfection with respiratory syncytial virus. Am J Dis Child. 1986; 140:543–546. [PubMed: 3706232]
6. Sigurs N, Gustafsson PM, Bjarnason R, Lundberg F, Schmidt S, Sigurbergsson F, Kjellman B. Severe respiratory syncytial virus bronchiolitis in infancy and asthma and allergy at age 13. Am J Respir Crit Care Med. 2005; 171:137–141. [PubMed: 15516534]

7. Lotz MT, Peebles RS Jr. Mechanisms of respiratory syncytial virus modulation of airway immune responses. Curr Allergy Asthma Rep. 2012; 12:380–387. [PubMed: 22692775]
8. Tripp RA, Oshansky C, Alvarez R. Cytokines and respiratory syncytial virus infection. Proc Am Thorac Soc. 2005; 2:147–149. [PubMed: 16113483]
9. Matsuse H, Hirose H, Tsuchida T, Fukahori S, Fukushima C, Mizuta Y, Kohno S. Effects of respiratory syncytial virus infection on dendritic cells and cysteinyl leukotrienes in lung tissues of a murine model of asthma. Allergol Int. 2007; 56:165–169. [PubMed: 17460444]
10. Hirose H, Matsuse H, Fukahori S, Tsuchida T, Tomari S, Kawano T, Fukushima C, Mizuta Y, Kohno S. Effects of repeated respiratory syncytial virus infections on pulmonary dendritic cells in a murine model of allergic asthma. Int Arch Allergy Immunol. 2008; 147:197–205. [PubMed: 18594149]
11. Tregoning JS, Yamaguchi Y, Harker J, Wang B, Openshaw PJ. The role of T cells in the enhancement of respiratory syncytial virus infection severity during adult reinfection of neonatally sensitized mice. J Virol. 2008; 82:4115–4124. [PubMed: 18272579]
12. Lukacs NW, Smit J, Lindell D, Schaller M. Respiratory syncytial virus-induced pulmonary disease and exacerbation of allergic asthma. Contrib Microbiol. 2007; 14:68–82. [PubMed: 17684333]
13. Palese P. Influenza: old and new threats. Nat Med. 2004; 10:S82–87. [PubMed: 15577936]
14. Webby RJ, Webster RG. Are we ready for pandemic influenza? Science. 2003; 302:1519–1522. [PubMed: 14645836]
15. Rothlin CV, Ghosh S, Zuniga EI, Oldstone MBA, Lemke G. TAM Receptors Are Pleiotropic Inhibitors of the Innate Immune Response. Cell. 2007; 131:1124–1136. [PubMed: 18083102]
16. Sharif MN, S. D. Rothlin CV, Kelly E, Lemke G, Olson EN, Ivashkiv LB. Twist mediates suppression of inflammation by type I IFNs and Axl. Journal of Experimental Medicine. 2006; 203:1891–1901. [PubMed: 16831897]
17. Scott RS, McMahon EJ, Pop SM, Reap EA, Caricchio R, Cohen PL, Earp HS, Matsushima GK. Phagocytosis and clearance of apoptotic cells is mediated by MER. Nature. 2001; 411:207–211. [PubMed: 11346799]
18. Lee WP, Liao Y, Robinson D, Kung HJ, Liu ET, Hung MC. Axl-gas6 interaction counteracts E1A-mediated cell growth suppression and proapoptotic activity. Mol Cell Biol. 1999; 19:8075–8082. [PubMed: 10567533]
19. Lemke G, Rothlin CV. Immunobiology of the TAM receptors. Nature Reviews Immunology. 2008; 8:327–336.
20. Chen J, C. K. Godowski PJ. Identification of Gas6 as a ligand for Mer, a neural cell adhesion molecule related receptor tyrosine kinase implicated in cellular transformation. Oncogene. 1997; 14:2033–2039. [PubMed: 9160883]
21. Fisher PW, B.-B. M. Wu SJ, Luo J, Carton J, Staquet K, Gao W, Jackson S, Bethea D, Chen C, Hu B, Giles-Komar J, Yang J. A novel site contributing to growth-arrest-specific gene 6 binding to its receptors as revealed by a human monoclonal antibody. Biochem. J. 2005; 1:727–735. [PubMed: 15579134]
22. Ohashi K. Identification of the Product of Growth Arrest-specific Gene 6as a Common Ligand for Axl, Sky, and Mer Receptor Tyrosine Kinases. Journal of Biological Chemistry. 1996; 271:30022–30027. [PubMed: 8939948]
23. Ekman C, Jonsen A, Sturfelt G, Bengtsson AA, Dahlback B. Plasma concentrations of Gas6 and sAxl correlate with disease activity in systemic lupus erythematosus. Rheumatology. 2011; 50:1064–1069. [PubMed: 21278074]
24. Jiang L, Liu CY, Yang QF, Wang P, Zhang W. Plasma Level of Growth Arrest-Specific 6 (GAS6) Protein and Genetic Variations in the GAS6 Gene in Patients With Acute Coronary Syndrome. American Journal of Clinical Pathology. 2009; 131:738–743. [PubMed: 19369636]
25. Mc Cormack O, Chung WY, Fitzpatrick P, Cooke F, Flynn B, Harrison M, Fox E, Gallagher E, Goldrick AM, Dervan PA, Mc Cann A, Kerin MJ. Growth arrest-specific gene 6 expression in human breast cancer. British Journal of Cancer. 2008; 98:1141–1146. [PubMed: 18283315]
26. Borgel D, Clauser S, Bornstain C, Bi??che I, Bissery A, Remones V. r. Fagon J-Y, Aiach M, Diehl J-L. Elevated growth-arrest-specific protein 6 plasma levels in patients with severe sepsis. Critical Care Medicine. 2006; 34:219–222. [PubMed: 16374177]

27. Fiebeler A, Park J-K, Muller DN, Lindschau C, Mengel M, Merkel S, Banas B, Luft FC, Haller H. Growth arrest specific protein 6/Axl signaling in human inflammatory renal diseases. American Journal of Kidney Diseases. 2004; 43:286–295. [PubMed: 14750094]

28. Angelillo-Scherrer A, d. F. P. Aparicio C, Melis E, Savi P, Lupu F, Arnout J, Dewerchin M, Hoylaerts M, Herbert J, Collen D, Dahlbäck B, Carmeliet P. Deficiency or inhibition of Gas6 causes platelet dysfunction and protects mice against thrombosis. Nature Medicine. 2001; 7:215–221.

29. Paccez JD, Vogelsang M, Parker MI, Zerbini LF. The receptor tyrosine kinase Axl in cancer: Biological functions and therapeutic implications. Int J Cancer. 2013

30. Paccez JD, Vasques GJ, Correa RG, Vasconcellos JF, Duncan K, Gu X, Bhasin M, Libermann TA, Zerbini LF. The receptor tyrosine kinase Axl is an essential regulator of prostate cancer proliferation and tumor growth and represents a new therapeutic target. Oncogene. 2013; 32:689–698. [PubMed: 22410775]

31. Hong J, Peng D, Chen Z, Sehdev V, Belkhiri A. ABL regulation by AXL promotes cisplatin resistance in esophageal cancer. Cancer Res. 2013; 73:331–340. [PubMed: 23117882]

32. Bosurgi L, Bernink JH, Delgado Cuevas V, Gagliani N, Joannas L, Schmid ET, Booth CJ, Ghosh S, Rothlin CV. Paradoxical role of the proto-oncogene Axl and Mer receptor tyrosine kinases in colon cancer. Proc Natl Acad Sci U S A. 2013; 110:13091–13096. [PubMed: 23878224]

33. Zhang Z, Lee JC, Lin L, Olivas V, Au V, LaFramboise T, Abdel-Rahman M, Wang X, Levine AD, Rho JK, Choi YJ, Choi CM, Kim SW, Jang SJ, Park YS, Kim WS, Lee DH, Lee JS, Miller VA, Arcila M, Ladanyi M, Moonsamy P, Sawyers C, Boggon TJ, Ma PC, Costa C, Taron M, Rosell R, Halmos B, Bivona TG. Activation of the AXL kinase causes resistance to EGFR-targeted therapy in lung cancer. Nat Genet. 2012; 44:852–860. [PubMed: 22751098]

34. Sullivan BM, Welch MJ, Lemke G, Oldstone MB. Is the TAM receptor Axl a receptor for lymphocytic choriomeningitis virus? J Virol. 2013; 87:4071–4074. [PubMed: 23325690]

35. Jemielity S, Wang JJ, Chan YK, Ahmed AA, Li W, Monahan S, Bu X, Farzan M, Freeman GJ, Umetsu DT, Dekruyff RH, Choe H. TIM-family proteins promote infection of multiple enveloped viruses through virion-associated phosphatidylserine. PLoS Pathog. 2013; 9:e1003232. [PubMed: 23555248]

36. Bhattacharyya S, Zagorska A, Lew ED, Shrestha B, Rothlin CV, Naughton J, Diamond MS, Lemke G, Young JA. Enveloped viruses disable innate immune responses in dendritic cells by direct activation of TAM receptors. Cell Host Microbe. 2013; 14:136–147. [PubMed: 23954153]

37. Meertens L, Carnec X, Lecoin MP, Ramdasi R, Guivel-Benhassine F, Lew E, Lemke G, Schwartz O, Amara A. The TIM and TAM families of phosphatidylserine receptors mediate dengue virus entry. Cell Host Microbe. 2012; 12:544–557. [PubMed: 23084921]

38. Morizono K, Xie Y, Olafsen T, Lee B, Dasgupta A, Wu AM, Chen IS. The soluble serum protein Gas6 bridges virion envelope phosphatidylserine to the TAM receptor tyrosine kinase Axl to mediate viral entry. Cell Host Microbe. 2011; 9:286–298. [PubMed: 21501828]

39. Mercer J. Viral apoptotic mimicry party: P.S. Bring your own Gas6. Cell Host Microbe. 2011; 9:255–257. [PubMed: 21501823]

40. Shimojima M, Takada A, Ebihara H, Neumann G, Fujioka K, Irimura T, Jones S, Feldmann H, Kawaoka Y. Tyro3 family-mediated cell entry of Ebola and Marburg viruses. J Virol. 2006; 80:10109–10116. [PubMed: 17005688]

41. Lukacs NW, Moore ML, Rudd BD, Berlin AA, Collins RD, Olson SJ, Ho SB, Peebles RS Jr. Differential immune responses and pulmonary pathophysiology are induced by two different strains of respiratory syncytial virus. Am J Pathol. 2006; 169:977–986. [PubMed: 16936271]

42. Ye X, Li Y, Stawicki S, Couto S, Eastham-Anderson J, Kallop D, Weimer R, Wu Y, Pei L. An anti-Axl monoclonal antibody attenuates xenograft tumor growth and enhances the effect of multiple anticancer therapies. Oncogene. 2010; 29:5254–5264. [PubMed: 20603615]

43. Hogaboam CM, Blease K, Mehrad B, Steinhauser ML, Standiford TJ, Kunkel SL, Lukacs NW. Chronic Airway Hyperreactivity, Goblet Cell Hyperplasia, and Peribronchial Fibrosis during Allergic Airway Disease Induced by Aspergillus fumigatus. The American Journal of Pathology. 2000; 156:723–732. [PubMed: 10666400]

44. Hussell T, Godlee A, Salek-Ardakani S, Snelgrove RJ. Respiratory viral infections: knowledge based therapeutics. Curr Opin Immunol. 2012; 24:438–443. [PubMed: 22770666]
45. Ye F, Han L, Lu Q, Dong W, Chen Z, Shao H, Kaplan HJ, Li Q. Retinal Self-Antigen Induces a Predominantly Th1 Effector Response in Axl and Mertk Double-Knockout Mice. The Journal of Immunology. 2011; 187:4178–4186. [PubMed: 21918185]
46. Maddox DM, Hicks WL, Vollrath D, LaVail MM, Naggert JK, Nishina PM. An ENU-Induced Mutation in the Mertk Gene (Mertknmf12) Leads to a Slow Form of Retinal Degeneration. Investigative Ophthalmology & Visual Science. 2011; 52:4703–4709. [PubMed: 21436282]
47. Wang Y, Moncayo G, Morin P Jr. Xue G, Grzmil M, Lino MM, Clement-Schatlo V, Frank S, Merlo A, Hemmings BA. Mer receptor tyrosine kinase promotes invasion and survival in glioblastoma multiforme. Oncogene. 2013; 32:872–882. [PubMed: 22469987]
48. Habibi MS, Openshaw PJ. Benefit and harm from immunity to respiratory syncytial virus: implications for treatment. Curr Opin Infect Dis. 2012; 25:687–694. [PubMed: 23086186]
49. Carrera Silva EA, Chan PY, Joannas L, Errasti AE, Gagliani N, Bosurgi L, Jabbour M, Perry A, Smith-Chakmakova F, Mucida D, Cheroutre H, Burstyn-Cohen T, Leighton JA, Lemke G, Ghosh S, Rothlin CV. T Cell-Derived Protein S Engages TAM Receptor Signaling in Dendritic Cells to Control the Magnitude of the Immune Response. Immunity. 2013; 39:160–170. [PubMed: 23850380]
50. Tate MD, Deng YM, Jones JE, Anderson GP, Brooks AG, Reading PC. Neutrophils ameliorate lung injury and the development of severe disease during influenza infection. J Immunol. 2009; 183:7441–7450. [PubMed: 19917678]
51. Sun J, Madan R, Karp CL, Braciale TJ. Effector T cells control lung inflammation during acute influenza virus infection by producing IL-10. Nat Med. 2009; 15:277–284. [PubMed: 19234462]
52. Tjwa M, B.-M. L. Lin Y, Lutgens E, Plaisance S, Bono F, Delesque-Touchard N, Hervé C, Moura R, Billiau AD, Aparicio C, Levi M, Daemen M, Dewerchin M, Lupu F, Arnout J, Herbert JM, Waer M, García de Frutos P, Dahlbäck B, Carmeliet P, Hoylaerts MF, Moons L. Gas6 promotes inflammation by enhancing interactions between endothelial cells, platelets, and leukocytes. Blood. 2008; 111:4096–4105. [PubMed: 18156494]
53. Gjerdrum C, Tiron C, Hoiby T, Stefansson I, Haugen H, Sandal T, Collett K, Li S, McCormack E, Gjertsen BT, Micklem DR, Akslen LA, Glackin C, Lorens JB. Axl is an essential epithelial-to-mesenchymal transition-induced regulator of breast cancer metastasis and patient survival. Proceedings of the National Academy of Sciences. 2009; 107:1124–1129.
54. Korns D, Frasch SC, Fernandez-Boyanapalli R, Henson PM, Bratton DL. Modulation of macrophage efferocytosis in inflammation. Front Immunol. 2011; 2:57. [PubMed: 22566847]
55. Lucas M, Stuart LM, Savill J, Lacy-Hulbert A. Apoptotic cells and innate immune stimuli combine to regulate macrophage cytokine secretion. J Immunol. 2003; 171:2610–2615. [PubMed: 12928413]
56. Stuart LM, Lucas M, Simpson C, Lamb J, Savill J, Lacy-Hulbert A. Inhibitory effects of apoptotic cell ingestion upon endotoxin-driven myeloid dendritic cell maturation. J Immunol. 2002; 168:1627–1635. [PubMed: 11823490]
57. Byrne A, Reen DJ. Lipopolysaccharide induces rapid production of IL-10 by monocytes in the presence of apoptotic neutrophils. J Immunol. 2002; 168:1968–1977. [PubMed: 11823533]
58. Fadok VA, Bratton DL, Konowal A, Freed PW, Westcott JY, Henson PM. Macrophages that have ingested apoptotic cells in vitro inhibit proinflammatory cytokine production through autocrine/paracrine mechanisms involving TGF-beta, PGE2, and PAF. J Clin Invest. 1998; 101:890–898. [PubMed: 9466984]
59. Finkelman FD, Hogan SP, Hershey GKK, Rothenberg ME, Wills-Karp M. Importance of Cytokines in Murine Allergic Airway Disease and Human Asthma. The Journal of Immunology. 2010; 184:1663–1674. [PubMed: 20130218]
60. Barlow JL, Bellosi A, Hardman CS, Drynan LF, Wong SH, Cruickshank JP, McKenzie ANJ. Innate IL-13–producing nuocytes arise during allergic lung inflammation and contribute to airways hyperreactivity. Journal of Allergy and Clinical Immunology. 2011
61. Seki Y, Inoue H, Nagata N, Hayashi K, Fukuyama S, Matsumoto K, Komine O, Hamano S, Himeno K, Inagaki-Ohara K, Cacalano N, O'Garra A, Oshida T, Saito H, Johnston JA, Yoshimura

A, Kubo M. SOCS-3 regulates onset and maintenance of T(H)2-mediated allergic responses. Nat Med. 2003; 9:1047–1054. [PubMed: 12847520]

62. Aoki T, Matsumoto Y, Hirata K, Ochiai K, Okada M, Ichikawa K, Shibasaki M, Arinami T, Sumazaki R, Noguchi E. Expression profiling of genes related to asthma exacerbations. Clin Exp Allergy. 2009; 39:213–221. [PubMed: 19187333]
63. Zhao J, Takamura M, Yamaoka A, Odajima Y, Iikura Y. Altered eosinophil levels as a result of viral infection in asthma exacerbation in childhood. Pediatr Allergy Immunol. 2002; 13:47–50. [PubMed: 12000498]

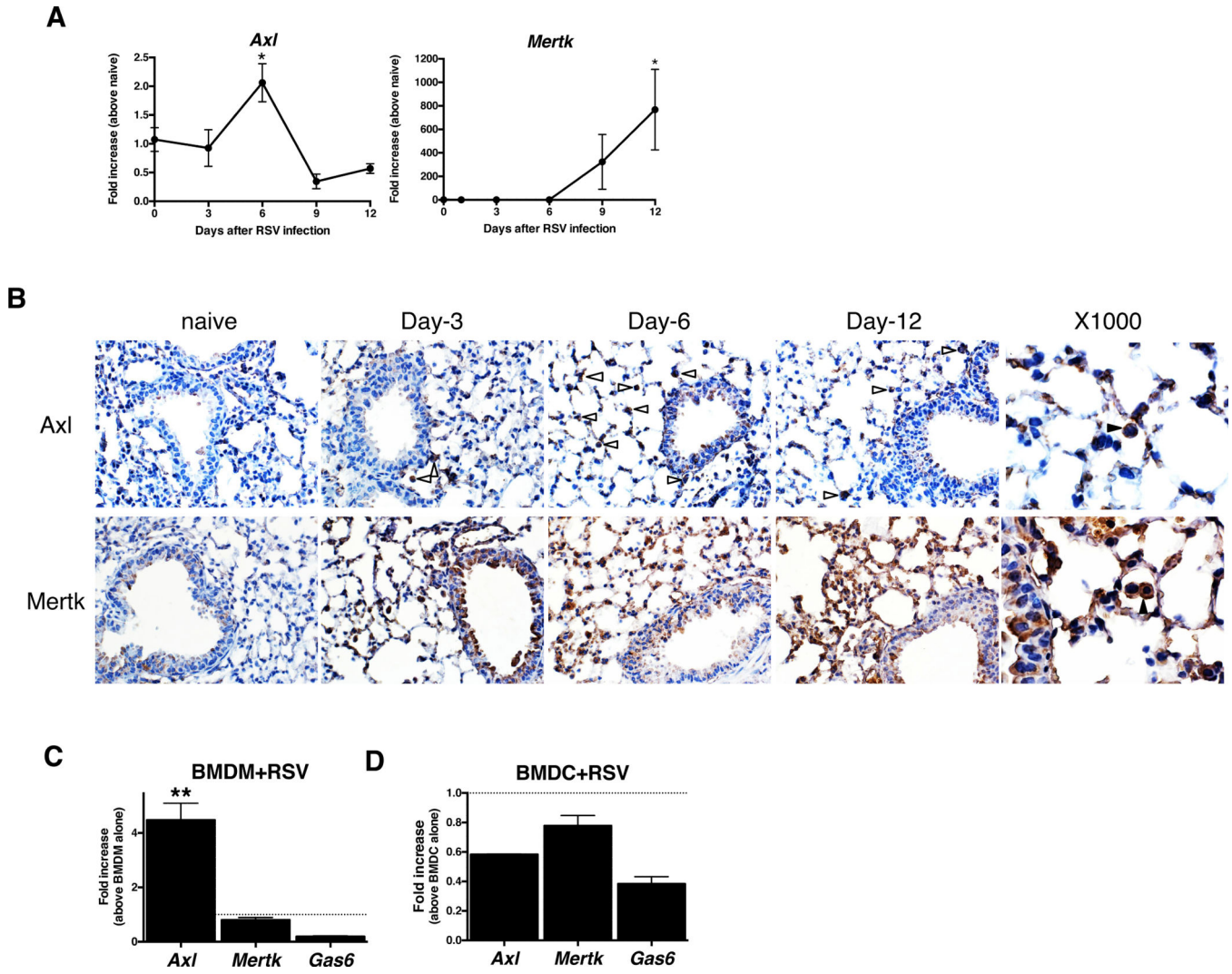

FIGURE 1. RSV infection induced Axl, and Mertk expression

Quantitative PCR analysis of whole lung transcript levels of *Axl* and *Mertk* prior to and at days 3, 6, 9, and 12 after RSV infection. *, $P<0.05$ versus the naïve group. Results are expressed as the mean ± SEM for n=5/group (**A**). Immunohistochemical analysis of Axl and Mertk in histological tissue sections from naïve and RSV-infected lung. Original magnification, ×400 and ×1000 (Axl at Day-6, Mertk at Day-12). Opened arrows indicate the Axl positive cells and solid arrow indicates Axl or Mertk-positive macrophage (**B**). Bone marrow-derived macrophages (BMDM) from naïve mice were exposed to RSV (1×10^4 PFU/ml) for 24 h and the transcript levels of *Axl* and *Mertk* were analyzed by q-PCR. **, $P<0.01$ versus PBS-treated macrophages (**C**). Bone marrow-derived dendritic cells (BMDC) from naïve mice were exposed to RSV for 24 hours and the transcript levels of *Axl* and *Mertk* were analyzed by q-PCR (**D**). Results are expressed as the mean ± SEM for n=5/group (**C**, **D**).

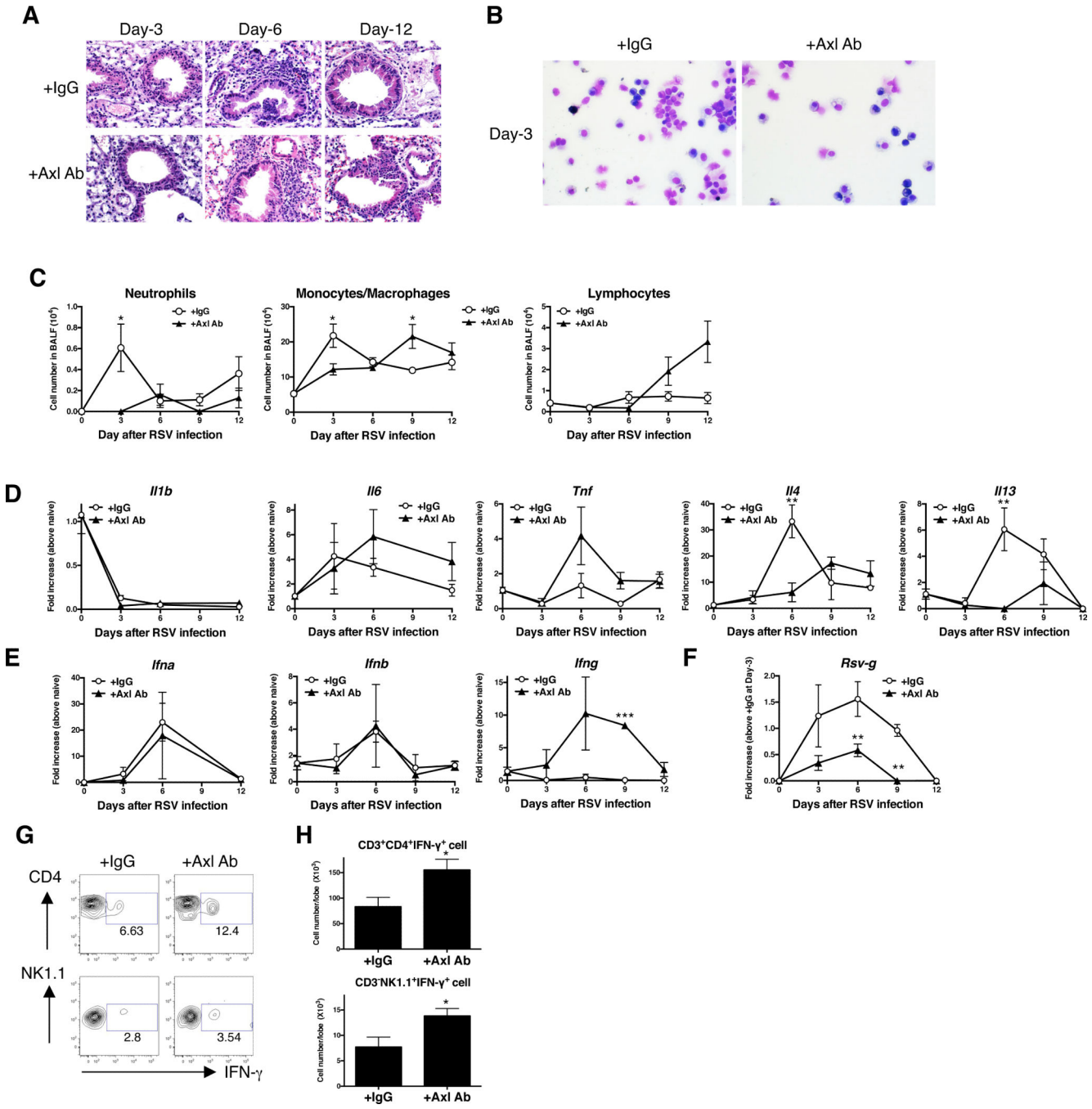

FIGURE 2. Anti-Axl mAb treatment attenuated RSV-induced histopathology

Mice were treated with IgG1 (+IgG1 Ab) or anti-Axl mAb (+Axl Ab) during primary RSV infection. Representative hematoxylin and eosin (H&E)-stained lung tissue sections from IgG1- (upper) and anti-Axl mAb-treated (lower) mice at days 3, 6, 12 after RSV infection. Original magnification, ×400 (**A**). Cytospin appearance of bronchoalveolar lavage fluid (BALF) harvested from IgG1- (upper) and Axl Ab-treated (lower) mice at days 3, 6, and 12 after RSV infection. Original magnification, ×400 (**B**). Quantification of neutrophils, monocytes/macrophages, and lymphocytes present in BALF samples at indicated times after

RSV infection. *P<0.05 compared with naïve mice (**C**). Quantitative real-time PCR analysis of *Il1b*, *Il6*, *tnfa*, *Il4*, and *Il13* at days 3, 6, 9, and 12 after RSV infection. *P<0.05, **P<0.01, **P<0.001 compared with IgG1-treated mice (**D**). Quantitative real-time PCR analysis of *Ifna*, *Ifnb*, *Ifng*, and *RSV-g* at days 3, 6, 9, and 12 after RSV infection. *P<0.05, **P<0.01, ***P<0.001 compared with naive mice (**E**). Representative flow cytometry data indicating IFN-γ-expressing CD4 T cells (upper panel) and NK cells (lower panel) in IgG1- and Axl Ab-treated lung at day-9 after primary RSV infection (**F**). The number of IFN-γ-producing CD4 T cells and IFN-γ-producing NK cells (lower panel) in IgG1- and Axl Ab-treated lung after RSV infection. *P<0.05, compared with IgG1-treated mice (**G**). Results are expressed as the mean ± SEM for n=5/group (**C-E, H**).

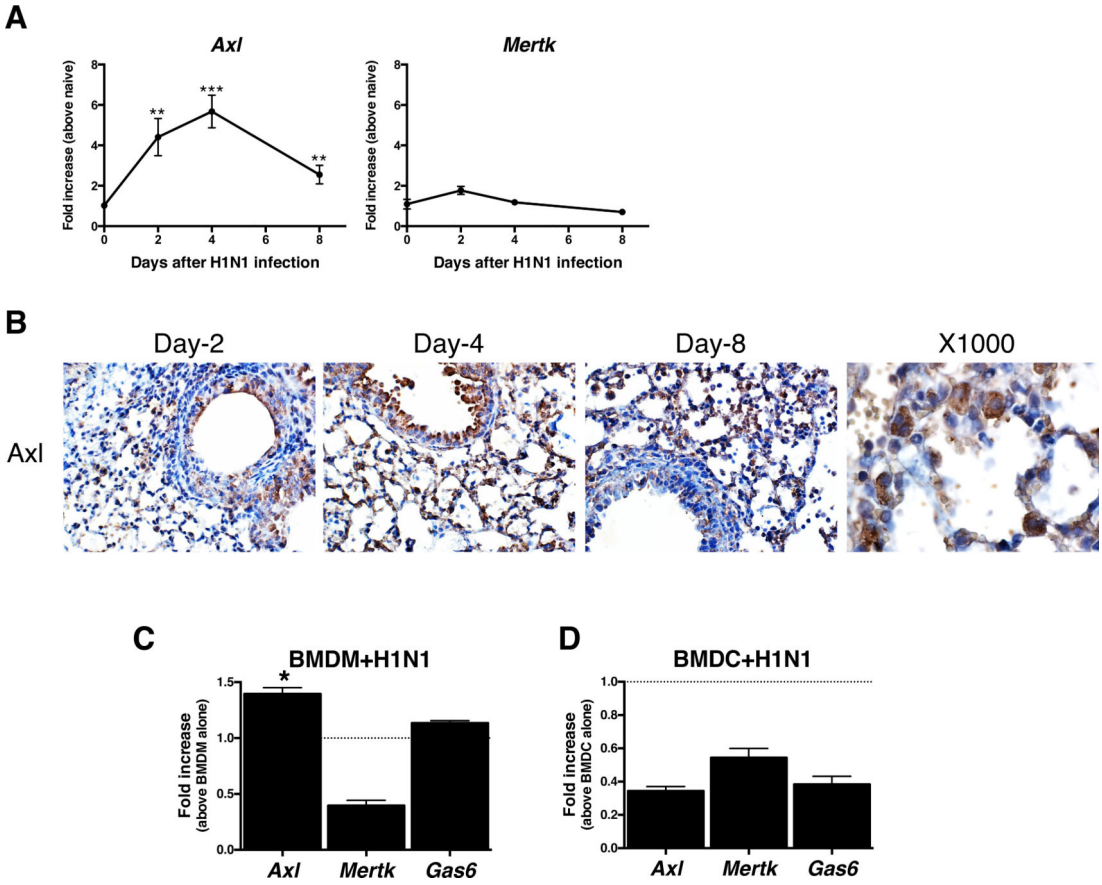

FIGURE 3. Primary H1N1 infection induced Axl expression in the lung

Quantitative PCR analysis of *Axl* and *Mertk* transcript levels in whole lung samples prior to and at days 2, 4, and 8 after H1N1 infection *, $P<0.05$, **, $P<0.01$ ***, $P<0.001$ versus the naïve group. Results are expressed as the mean ± SEM of n=5/group (**A**). Temporal immunohistochemical analysis of airway (top panels) and interstitial (bottom panels) expression of Axl in lung tissue sections from naïve and H1N1-infected mice. Original magnification, ×400 and ×1000 (at Day-4) (**B**). Bone marrow-derived macrophages (BMDM) from naïve mice were exposed to H1N1 for 24 h, and the transcript levels of *Axl* and *Mertk* were determined using q-PCR (**C**). Bone marrow-derived dendritic cells (BMDC) from naïve mice were exposed to H1N1 (MOI=10) for 24 h, and the transcript levels of *Axl* and *Mertk* were determined using q-PCR (**D**). **, $P<0.01$ versus PBS-treated macrophages (mean value indicated by dotted line). Results are expressed as the mean ± SEM for n=3/group (**C**, **D**).

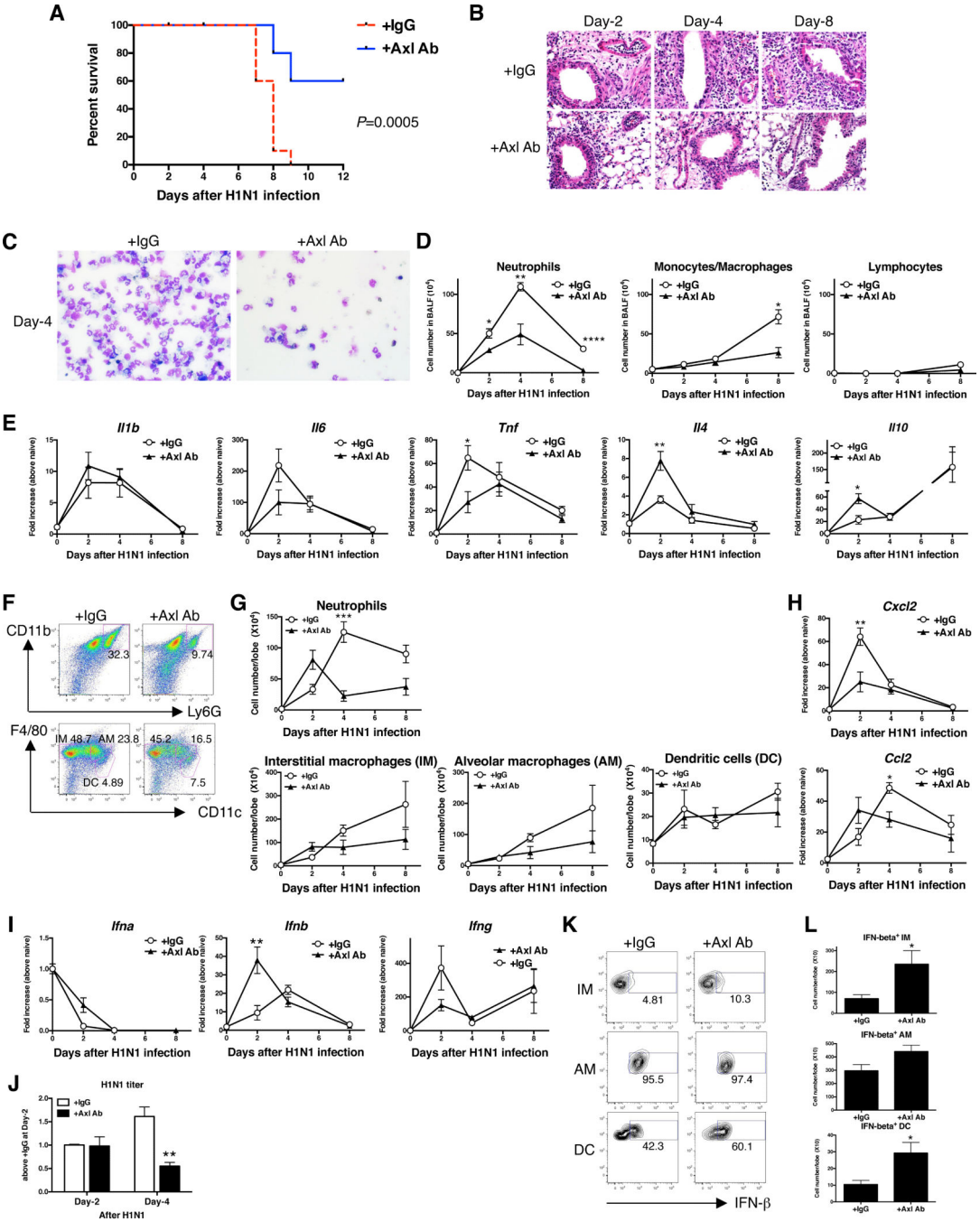

FIGURE 4. Anti-Axl mAb treatment inhibited influenza-induced lethality and histopathology

Mice were treated with IgG1 (+IgG1 Ab) or anti-Axl mAb (+Axl Ab) prior to and during H1N1 infection. Kaplan Meier survival plot of IgG1-treated and Axl mAb-treated mice during H1N1 infection (**A**). Results are expressed as the percent of survival of a starting cohort of 10 mice per group. Representative H&E-stained lung tissue sections from IgG1- and Axl Ab-treated mice at days 2, 4, and 8 after H1N1 infection. Original magnification, ×400 (**B**). Cellular cytospin appearance of BAL harvested from IgG1- and anti-Axl mAb-treated mice. Original magnification, ×400 (**C**). Quantification of neutrophils, monocytes/

macrophages, and lymphocytes harvested in BALF from IgG1- and anti-Axl mAb-treated mice (**D**). Quantitative PCR analysis of *Il1b*, *Il6*, *tnfa*, *Il4*, and *Il10* (**E**). Representative flow cytometry analysis of neutrophils, interstitial macrophages (IM), alveolar macrophages (IM), and dendritic cells (DC) in IgG1- and Axl Ab-treated lung at day 4 after H1N1 infection (**F**). Quantification of neutrophils, IM, AM, and DC in IgG1- and anti-Axl mAb-treated lung after H1N1 infection (**G**). Quantitative PCR analysis of *Cxcl2*, *Ccl2* (**H**), and *Ifn-b* (**I**). Lung viral titers in IgG1- and anti-Axl mAb-treated mice at days 2 and 4 after H1N1 infection (**J**). Representative flow cytometry analysis of IFN-β-producing IM, AM, and DC in IgG1- and anti-Axl mAb-treated lung at day 2 after H1N1 infection (**K**). Quantification of IFN-β-producing IM, AM, and DC in IgG1- and anti-Axl mAb-treated lung after H1N1 infection in naïve mice (**L**). Results are expressed as the mean ± SEM for n=2-5/group. *P<0.05, **P<0.01, ***P<0.001, ****P<0.0001 compared with IgG-treated group (D, E, G, H, I, K).

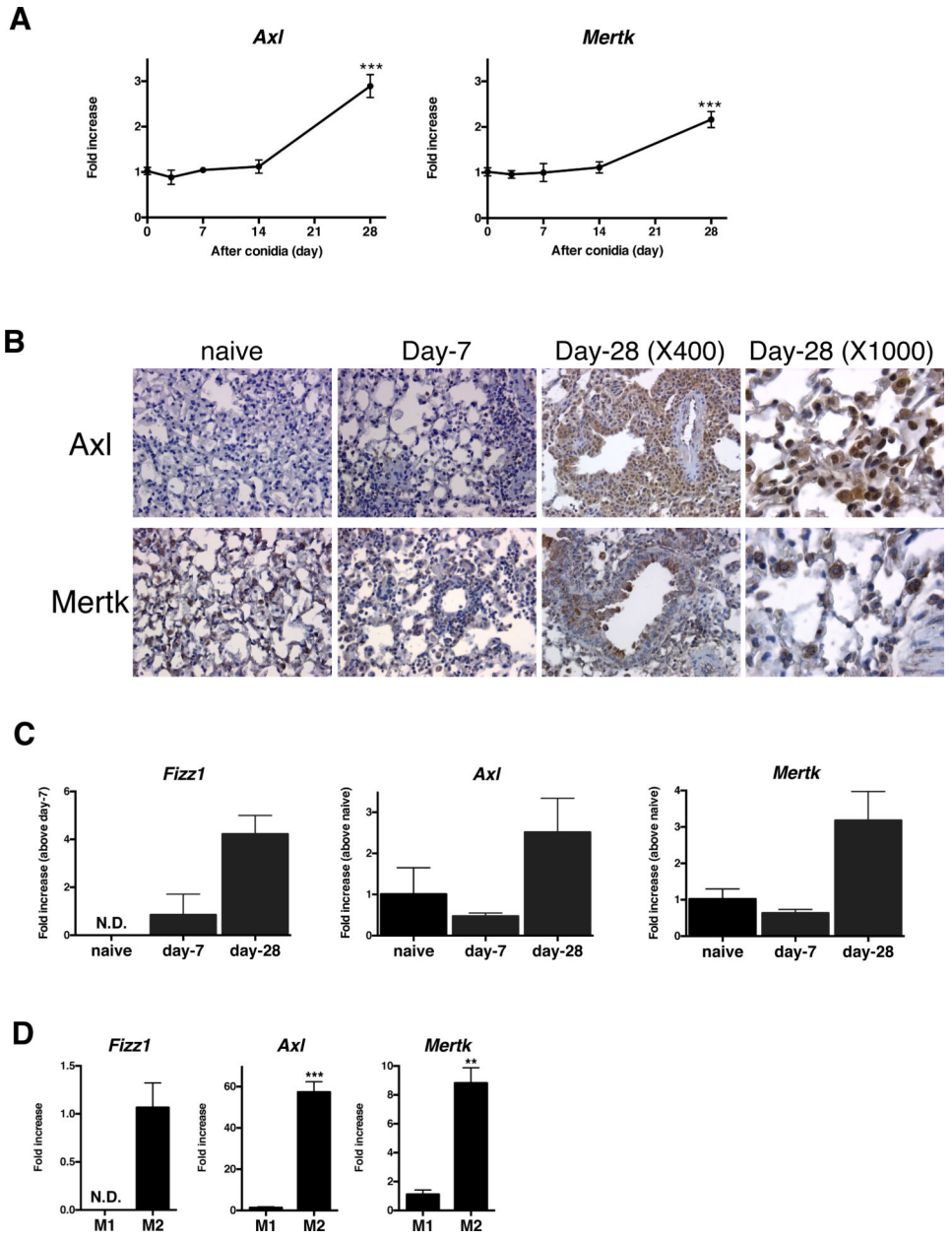

FIGURE 5. Axl and Mertk expression during chronic fungal asthma in mice

Quantitative analysis of transcript levels of *Axl* and *Mertk* in whole lung samples prior to and at days 3, 7, 14, and 28 after *Aspergillus fumigatus* conidia challenge to *A. fumigatus*-sensitized mice. ***, $p<0.01$ versus naïve mice(**A**). Representative immunohistochemical analysis of Axl and Mertk expression (brown) in tissue sections from naïve and asthmatic mice (**B**). Quantitative PCR analysis of *Fizz1*, *Axl*, and *Mertk* in bone marrow-derived macrophages (BMDM) from naïve mice and asthmatic mice prior to and at days 7 and 28 after conidia *, $P<0.05$ versus naïve macrophages (**C**). Quantitative PCR analysis of *Fizz1*, *Axl*, and *Mertk* in LPS/IFN-γ-induced M1 macrophages (M1) and IL-4/IL-13-induced M2 macrophages (M2). ***, $P<0.001$ versus M1 (**D**). Results are expressed as the mean ± SEM for n=5/group (**A**, **C**). Results are expressed as the mean ± SEM for n=3/group (**D**).

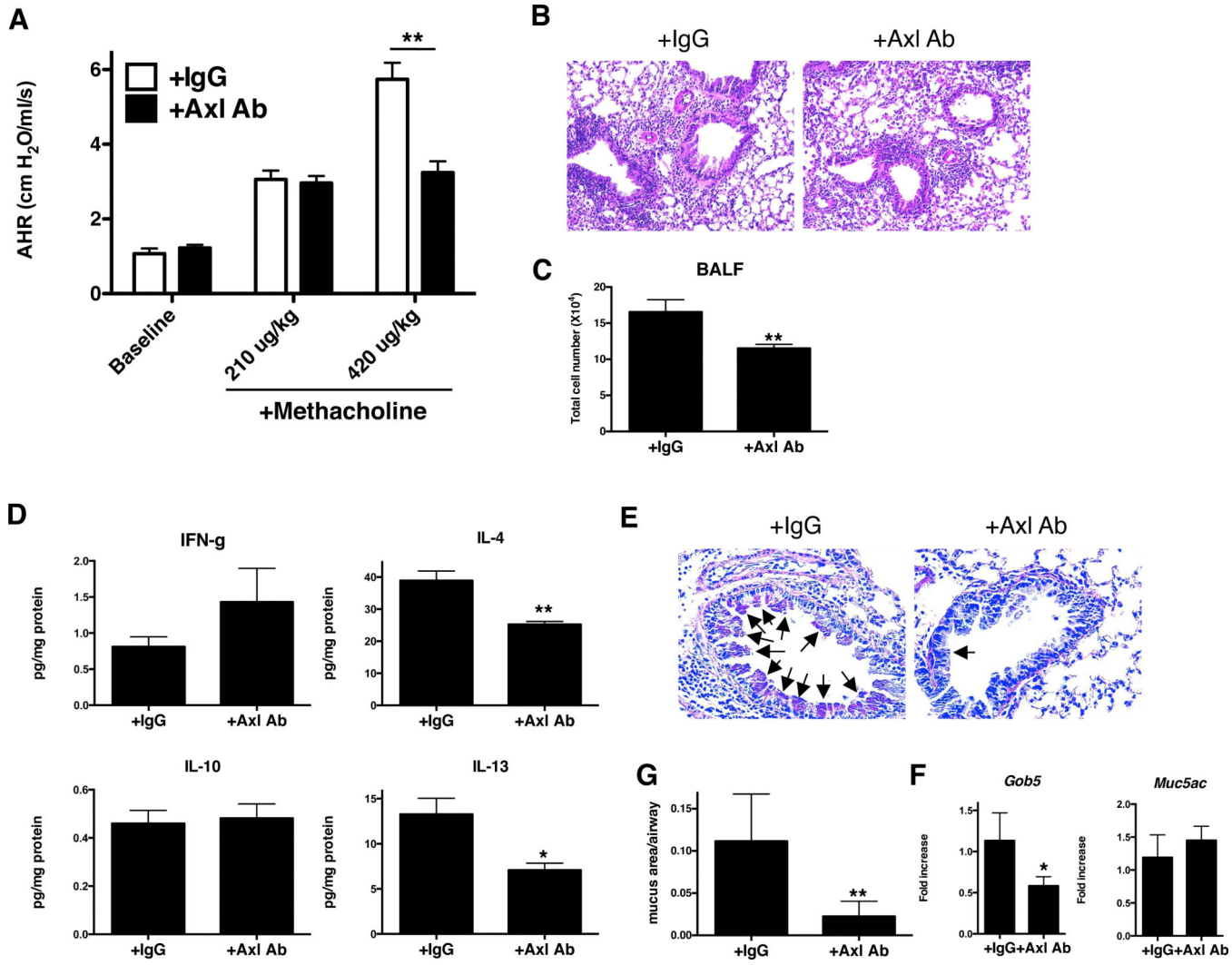

FIGURE 6. Axl activity contributes to airway hyperresponsiveness, inflammation, and remodeling in an experimental fungal asthma model

Airway hyperresponsiveness to a dose of 210 μg/kg or 420 μg/kg of methacholine in IgG1-treated (+IgG1) or anti-Axl mAb-treated (+Axl mAb; 5 μg/dose i.p. × 7 doses; **A**) at day 28 after conidia. Representative H&E-stained lung tissue sections from both treatment groups at day 28 after conidia (**B**). Quantification of cells present in BALF from IgG1- and anti-Axl mAb-treated asthmatic mice **P<0.01 compared with naïve mice (**C**). Whole lung protein levels of IFN-γ, IL-4, IL-10, and IL-13 in asthmatic mice treated with IgG1 or anti-Axl mAb at day 28 after conidia (**D**). Representative PAS-stained lung tissue sections from the IgG1 and anti-Axl mAb groups at day 28 after conidia (**E**). Quantitative analysis of mucus area in airway from IgG1- and Axl Ab-treated groups at day 28 after conidia (**F**). Arrows indicate the mucus-producing cells in the airway epithelium. Quantitative PCR analysis of *Muc5ac* and *Gob5* in the IgG1 and anti-Axl mAb groups at day 28 after conidia (**G**). Results are expressed as the mean ± SEM for n=5/group. *, $p<0.05$, **, $p<0.01$ vs. control (indicated as IgG).

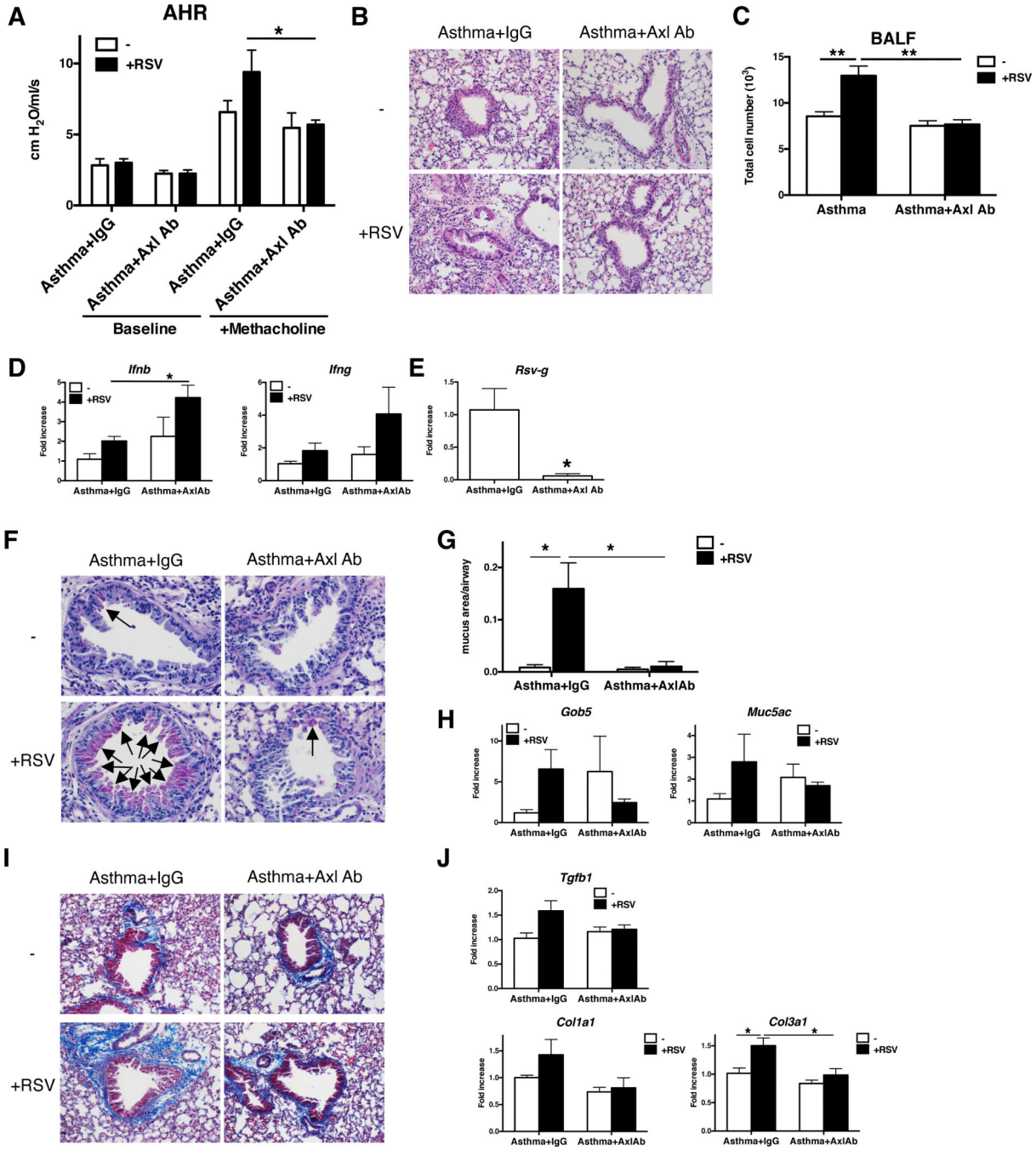

FIGURE 7. Axl activity promotes airway hyperresponsiveness, inflammation, and remodeling in RSV-exacerbated fungal asthma

Airway hyperresponsiveness to a dose of 210 μg/kg or 420 μg/kg of methacholine in IgG1-treated (+IgG1) or anti-Axl mAb-treated (+Axl mAb; 5 μg/dose i.p. × 7 doses) RSV-infected asthmatic mice (at day 42 after conidia challenge or day 12 after RSV infection) (**A**). Representative H&E-stained lung tissue sections from all treatment groups at day 42 after conidia with mock (−) or RSV infection (+) (**B**). Quantification of cell counts in BALF from IgG1- and Axl Ab-treated asthmatic mice with (+) and without (−) RSV. **P<0.01 (**C**).

Quantitative real-time PCR analysis of *Ifnb* and *Ifng* (**D**), and *RSV-g* (**E**) at day 42 after conidia challenge with mock (−) or RSV infection (+). *P<0.05. Representative PAS-stained lung tissue sections from IgG1- and Axl Ab-treated mice at day 42 after conidia with mock (−) or RSV infection (+) (**F**). Arrows indicate the mucin-producing cells in the airway epithelium. Quantitative histologic analysis of mucus area in all treatment groups (**G**). Quantitative PCR analysis of *Muc5ac* and *Gob5* in IgG1- and ant-Axl mAb-treated asthmatic mice at day 42 after conidia with mock (−) or RSV infection (+) (**H**). Representative Masson trichrome-stained lung tissue sections from IgG1- and anti-Axl mAb-treated asthmatic mice at day 42 after conidia with mock (−) or RSV infection (+) (**I**). Light blue staining indicates the presence of extracellular matrix including collagen, which is an index of airway remodeling. Quantitative PCR analysis of *Tgfb1*, *Col1a1*, and *Col3a1* at day 42 after conidia with mock (−) or RSV infection (+) (**J**). Results are expressed as the mean ± SEM for n=5/group.